NANO LETTERS

Letter

pubs.acs.org/NanoLett

Plateau–Rayleigh Crystal Growth of Nanowire Heterostructures: Strain-Modified Surface Chemistry and Morphological Control in One, Two, and Three Dimensions

Robert W. Day,[†] Max N. Mankin,[†] and Charles M. Lieber*[,†,‡]

[†]Department of Chemistry and Chemical Biology and [‡]Harvard John A. Paulson School of Engineering and Applied Sciences, Harvard University, Cambridge, Massachusetts 02138, United States

Supporting Information

ABSTRACT: One-dimensional (1D) structures offer unique opportunities for materials synthesis since crystal phases and morphologies that are difficult or impossible to achieve in macroscopic crystals can be synthesized as 1D nanowires (NWs). Recently, we demonstrated one such phenomenon unique to growth on a 1D substrate, termed Plateau–Rayleigh (P-R) crystal growth, where periodic shells develop along a NW core to form diameter-modulated NW homostructures with tunable morphologies. Here we report a novel extension of the P-R crystal growth concept with the synthesis of heterostructures in which Ge (Si) is deposited on Si (Ge) 1D cores to generate complex NW morphologies in 1, 2, or 3D. Depositing Ge on 50 nm Si cores with a constant GeH_4 pressure yields a single set of periodic shells, while sequential variation of GeH_4 pressure can yield multimodulated 1D NWs with two distinct sets of shell periodicities. P-R crystal growth on 30 nm cores also produces 2D loop structures, where Ge (Si) shells lie primarily on the outside (inside) of a highly curved Si (Ge) core. Systematic investigation of shell morphology as a function of growth time indicates that Ge shells grow in length along positive curvature Si cores faster than along straight Si cores by an order of magnitude. Short Ge deposition times reveal that shells develop on opposite sides of 50 and 100 nm Si cores to form straight 1D morphologies but that shells develop on the same side of 20 nm cores to produce 2D loop and 3D spring structures. These results suggest that strain mediates the formation of 2 and 3D morphologies by altering the NW's surface chemistry and that surface diffusion of heteroatoms on flexible freestanding 1D substrates can facilitate this strain-mediated mechanism.

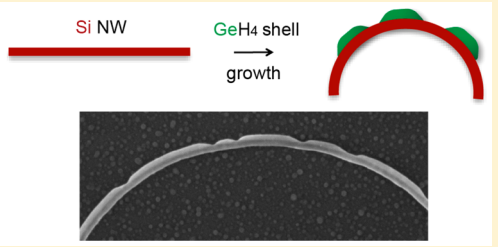

KEYWORDS: *Core/shell synthesis, diameter-modulated nanowire, tensile/compressive stress, silicon, germanium heteroepitaxy, compliant, freestanding substrate*

The unique properties of 1D NW materials[1−4] have the potential to enable fundamental scientific discoveries as well as transform many areas of technology.[5−12] For example, NWs have had an important impact on areas ranging from energy conversion,[5,6] thermal,[7] and optical[8] applications, to powerful tools for biology.[9,10] The realization of these scientific and technological pursuits depends critically on the ability to control the NW's structure and thus properties through synthesis. To this end, efforts have focused on primarily two synthetic paradigms where the morphology, composition, and crystal structure can be controlled either along the NW axis during growth[13] or radially during sequential core/shell growth.[5] Significant advances have been made by better understanding the detailed mechanisms of established synthetic approaches, most notably the nanocluster-catalyzed vapor–liquid–solid (VLS) mechanism.[13] 1D structures also present unique opportunities for materials synthesis since crystal phases and morphologies that are difficult to obtain or which have no equivalent counterpart in 0D, 2D or bulk configurations, have been synthesized in NWs, including hexagonal Si,[14] embedded quantum dots,[15,16] kinked NWs,[17,18] polytypic and twin-plane superlattices,[19] and an emerging class of structures, diameter-modulated NWs.[9,20−24]

To this end, we recently demonstrated a new synthetic paradigm unique to 1D substrates[23] termed P-R crystal growth and showed that this new approach could be used to synthesize diameter-modulated core/shell NWs in which the modulation is tunable in both axial and radial directions. Much of the literature describing homoepitaxial growth of core/shell NWs has yielded radially conformal shells continuous along the NW axis[5] as expected in analogy to 2D homoepitaxial thin film growth.[25] In P-R crystal growth,[23] radial growth can spontaneously produce periodic shells, which are noncontinuous along the length of the NW. Borrowing concepts from the P-R instability and with straightforward geometric arguments, we illustrated how diameter-modulated NWs can have less total surface energy than uniform diameter NWs, which consequently drives their formation. The kinetics of growth,

Received: February 12, 2016
Revised: February 26, 2016
Published: March 1, 2016

ACS Publications © 2016 American Chemical Society

DOI: 10.1021/acs.nanolett.6b00629
Nano Lett. 2016, 16, 2830−2836

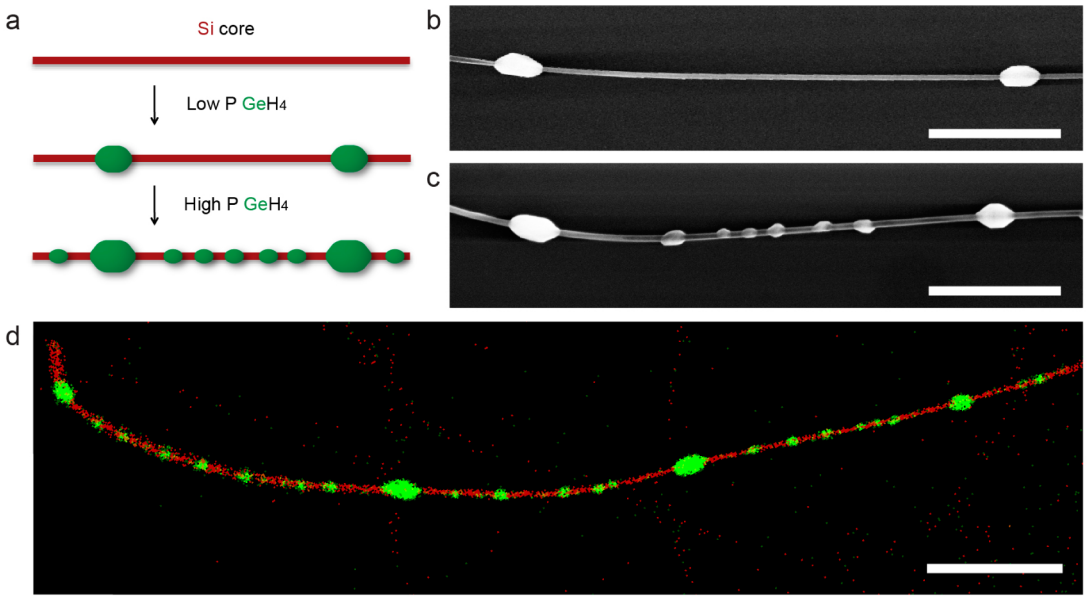

Figure 1. P-R crystal growth of periodic shell heterostructures. (a) Schematic depicting single-step (middle) and two-step (bottom) synthesis of Ge periodic shells on a Si NW core (top). (b, c) SEM images of NWs following (b) single- and (c) two-step Ge deposition on 50 nm diameter Si NWs at 480 °C. Ge shells were grown for 80 min with 1 sccm (0.48 mTorr) GeH_4 in the single-step growth (b), and for 80 min with 1 sccm (0.48 mTorr) GeH_4 followed by 2.5 min with 40 sccm (19 mTorr) GeH_4 in the two-step growth (c). (d) Scanning transmission electron microscopy (STEM) energy-dispersive X-ray spectroscopy (EDS) elemental mapping of Si (red) and Ge (green) of NW grown with same two-step shell deposition conditions as in c. Scale bars are 1 μm.

however, determines whether P-R crystal growth can occur and affords tunability over various morphological features. Specifically, for our chemical vapor deposition (CVD) growth studies of Si shells on Si cores, and Ge shells on Ge cores, the diffusion lengths for surface adatoms must be sufficiently long with respect to NW core diameter so that shell material can spontaneously assemble into distinct periodic shells and grow nonuniformly along a NW's length.[23]

Here, we extend P-R crystal growth to heterostructures by growing Ge periodic shells on Si cores and Si periodic shells on Ge cores. Combining different materials to form heterostructures is a powerful means of tuning material properties through, for example, considerations of band alignment[26] and strain.[27] Strain has been shown to influence the morphology of core/shell nanowire heterostructures in 1D,[28−31] and also more broadly, to drive the formation of curved 3D structures in biology.[32] By controlling the shell growth conditions and the diameter of the core, we demonstrate that P-R crystal grow of heterostructures can form complex NW morphologies in 1, 2, and 3D. We performed systematic growth studies as a function of time and with different core diameters to understand the mechanism driving the formation of these complex structures.

Initially, we focused on single and two-step growth of Ge periodic shells on Si cores since these would be expected to produce one and two distinct diameter-modulations, respectively, on 1D Si NW cores (Figure 1a) according to our homoepitaxial P-R crystal growth model.[23] In brief, Si NW cores were grown by the Au-catalyzed VLS mechanism in a home-built CVD chamber (see Materials and Methods in Supporting Information). Then, for the single-step growth, the temperature was increased to 480 °C and the total pressure reduced to 0.3 Torr, at which point GeH_4 was introduced with flow rate of 1 sccm (0.48 mTorr) for 80 min. A representative scanning electron microscopy (SEM) image (Figure 1b) of a NW from this growth reveals radially conformal Ge periodic shells on a 50 nm Si core where initial Ge and Si composition assignments are based on contrast differences and previous work.[23] The Ge shells produced had an average diameter of 190 nm with an average periodic spacing, or pitch, of 3.6 μm.

In the two-step process, Ge shells were first grown for 80 min with 1 sccm (0.48 mTorr) GeH_4 as described above, and then a second growth step was carried out at a higher GeH_4 flow rate of 40 sccm (19 mTorr) for 2.5 min. SEM images of NWs resulting from sequential in situ variations in Ge shell growth conditions (Figure 1c) revealed two distinct sets of roughly periodic Ge shells with average diameters/pitches of 160 nm/3.1 μm and 100 nm/480 nm, respectively. In addition, scanning transmission electron microscopy (STEM) energy-dispersive X-ray spectroscopy (EDS) elemental mapping data of a NW obtained using the same sequential two-step Ge shell deposition conditions (Figure 1d) confirm the material assignments of the core as Si (red) and periodic shells as Ge (green) and illustrates the two distinct nearly periodic modulations.

As a control, single-step Ge shell growth using the "second-step" conditions (i.e., GeH_4 flow rate of 40 sccm (19 mTorr) for 2.5 min) yielded only a single set of periodic shells (Supporting Information, Figure S1) with average diameter of 90 nm and pitch of 360 nm, respectively. These periodic Ge shells have a modulation amplitude and periodicity very similar to the second set seen in Figure 1c. These longer/shorter periodicity results, which were obtained at lower/higher GeH_4 flow (and partial pressure), highlight that periodic shell pitch can be controlled by growth conditions as described in our previous homoepitaxial studies of P-R crystal growth.[23] Specifically, longer pitch shells (Figures 1b, c) are obtained for longer diffusion lengths of Ge adatoms at lower deposition pressures, while the shorter pitch shells develop due to shorter diffusion lengths at higher deposition pressures.[23] Comparing the dimensions of the larger, longer pitch shells and the smaller,

DOI: 10.1021/acs.nanolett.6b00629
Nano Lett. 2016, 16, 2830−2836

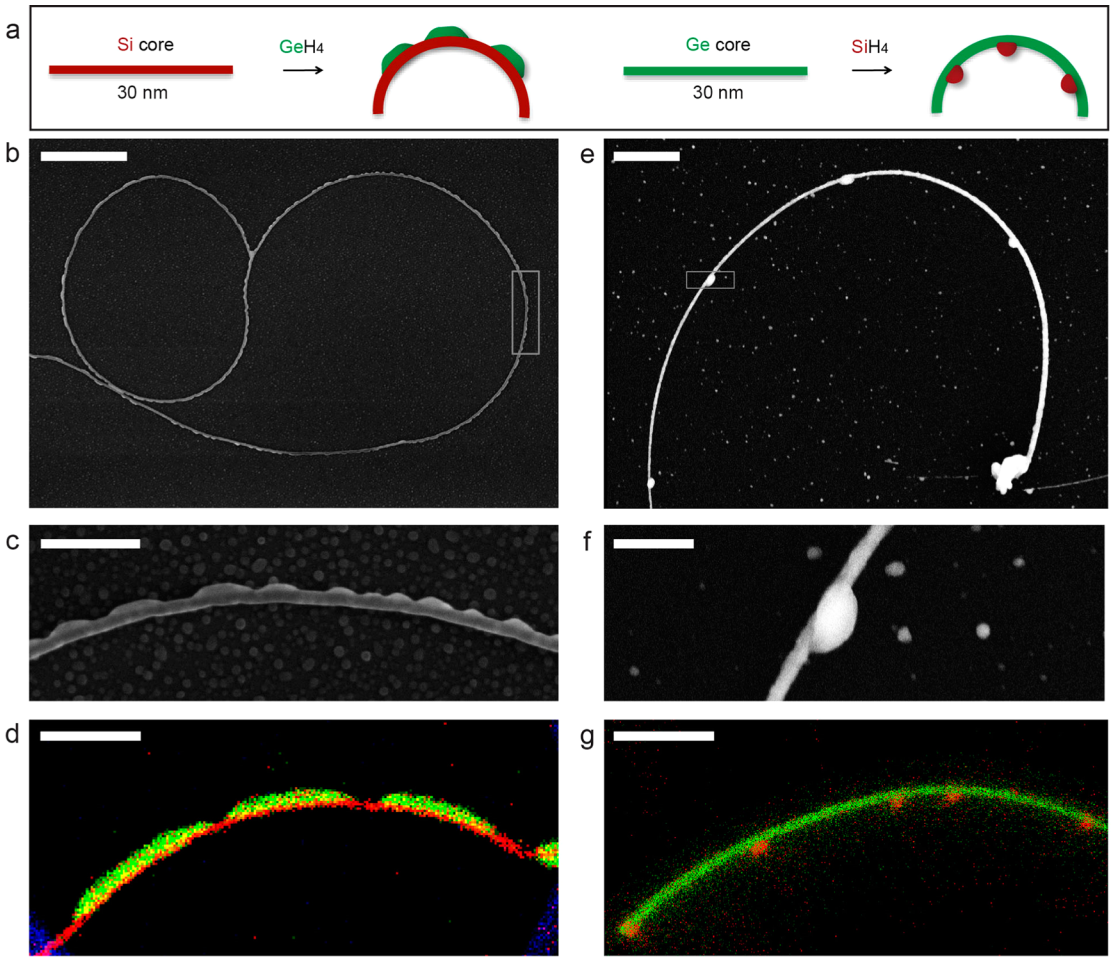

Figure 2. P-R crystal growth of nonconformal periodic shell heterostructures on small diameter NWs. (a) Left, schematic of periodic Ge shell growth on the outer surface of a curved Si NW core; right, schematic of periodic Si shell growth on the inner surface of a curved Ge NW core. (b) SEM image of a NW after Ge deposition on a 30 nm Si core at 520 °C and 40 sccm (19 mTorr) GeH_4 for 30 s. Scale bar: 1 μm. (c) SEM image from open rectangular box (right) in (b). Scale bar: 200 nm. (d) STEM EDS map of Ge (green) shells on a Si (red) NW core on carbon (blue) grid. Scale bar: 300 nm. (e) SEM image of a NW after Si deposition on a 30 nm Ge NW core at 680 °C with 0.8 sccm (3.6 mTorr) SiH_4 for 28 min. Scale bar: 1 μm. (f) SEM image from open rectangular box (left) in e. Scale bar: 250 nm. (g) STEM EDS map of Si (red) shells on a Ge (green) core. Scale bar: 600 nm.

shorter pitch shells from the multistep deposition structure (Figure 1c) with the dimensions of the lower pressure (Figure 1b) and higher pressure (Supporting Information, Figure S1) single-step deposition structures, respectively, supports our interpretation.

To further understand key factors affecting growth of the heterostructure periodic shells, which should have strained interfaces due to lattice mismatch,[25] we carried out experiments using smaller diameter NWs (Figure 2). The increased NW flexibility with decreasing diameter[33] suggests the possibility of curved 2D structures, where periodic shell growth occurs on one "side" of the NW in a way that reduces interfacial stress. Specifically, Ge (Si) periodic shells grow on the outer (inner) surface of curved Si (Ge) NW cores as shown schematically in Figure 2a.

Notably, SEM images of NWs obtained from Ge deposition on 30 nm Si cores at 520 °C with 40 sccm (19 mTorr) GeH_4 for 30 s (e.g., Figure 2b) revealed curved NWs with 2D loop morphologies; key structural features include the following. First, the looped NW and substrate are in focus (Figure 2b) indicating that the 2D morphology lies within the <1 μm SEM depth of field for these imaging conditions. Second, contrast differences in magnified portions of this SEM image (e.g., Figure 2c) indicate that these Ge shells are not conformal around the NW core in contrast to the radially conformal periodic shells of Figure 1. Third, quantitative analysis shows that >95% of all shells lie on the outer surface of these curved Si NW cores. In addition, elemental mapping analysis by STEM EDS (Figure 2d) confirms that Ge shells (green) lie on the outside of curved Si cores (red).

We also deposited Si onto similar diameter Ge NW cores using higher temperature/lower pressure conditions than used previously to produce continuous radially conformal Si shells.[34] SEM images of NWs obtained from Si deposition on 30 nm Ge cores at 680 °C with 0.8 sccm (3.6 mTorr) SiH_4 for 28 min (Figure 2e) revealed curved 2D morphologies. Significantly, the contrast in these images (Figure 2e,f) suggest that the periodic Si shells lie on the inner surface of the curved Ge core. STEM EDS mapping (Figure 2g) confirm the material assignments of the periodic Si shells (red) on the inner surface of the Ge (green) NW core.

The formation of curved 2D morphologies from periodic shell heterostructure growth can be understood in the context of lattice mismatched heteroepitaxy. Heteroepitaxy of Ge (Si)

DOI: 10.1021/acs.nanolett.6b00629
Nano Lett. 2016, 16, 2830−2836

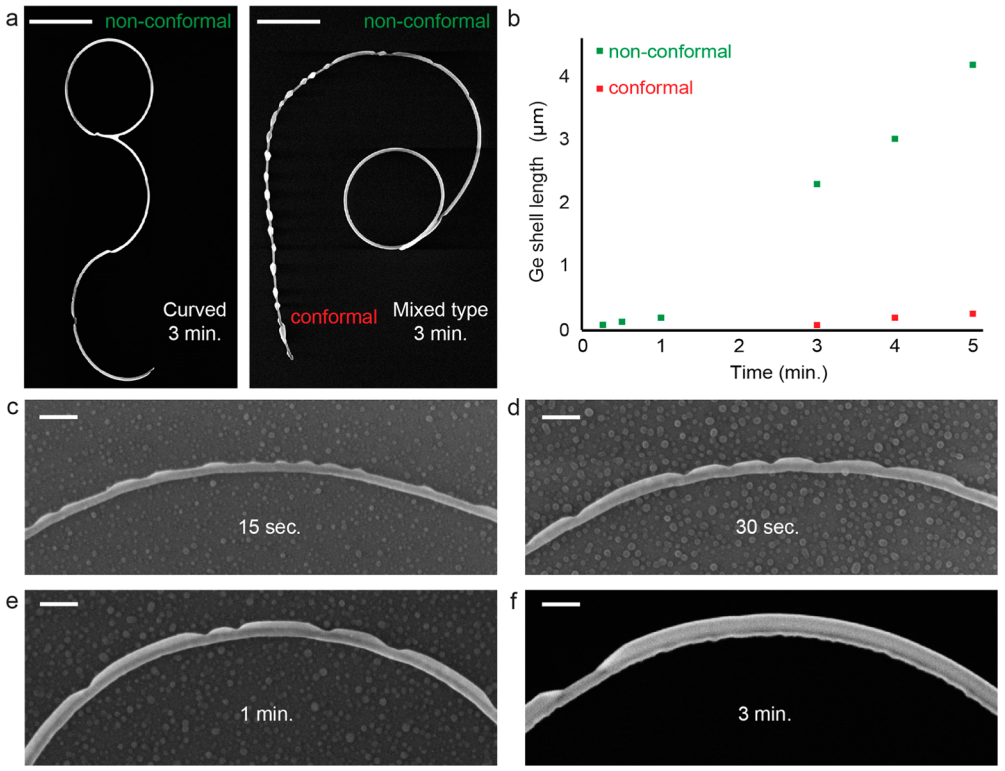

Figure 3. P-R crystal growth of Ge periodic shells on Si NW cores as a function of growth time. (a) SEM images of NWs after 3 min of shell growth having 2D curved morphologies with shells only on the outer surface of a curved NW (nonconformal, left), and mixed morphology with both nonconformal and conformal shells (right). Scale bars: 1 μm. (b) Average Ge shell lengths along the core as a function of shell growth time. SEM was used to measure the lengths of nonconformal (green) and conformal (red) Ge shells on NWs having mixed type morphology. (c–f) Representative SEM images obtained from Ge shells on curved cores after 0.25 (c), 0.5 (d), 1 (e), and 3 min (f). Scale bars: 100 nm. For all growths Ge was deposited on 30 nm Si cores at 520 °C with 40 sccm (19 mTorr) GeH_4. Representative SEM images for NW and shell morphologies for all times are shown in Supporting Information.

on bulk and 2D Si (Ge) substrates can lead to compressive and tensile strain of Ge and Si, respectively, at the interface to accommodate the 4% lattice mismatch.[25,35−39] Surface stress on one side of a substrate can induce bending.[25,39] Assuming that Ge and Si are under compressive and tensile stress, respectively, at the interface of our nonconformal shells, a tensile (compressive) stress on one side of the Si (Ge) core will bend the NW away from (toward) the shells. Hence, the observed morphologies with periodic Ge shells on the outer curved surface of Si NW cores and periodic Si shells on the inner curved surface of Ge NW cores are consistent with this picture of accommodating lattice mismatch by bending the NW "substrate".

To better understand the development of the curved NW heterostructures, we further characterized the morphologies of NWs and individual shells on NWs as a function of shell growth time (Figure 3). In six separate syntheses, Ge was deposited on 30 nm Si cores at 520 °C with 40 sccm (19 mTorr) GeH_4 for 0.25, 0.5, 1, 3, 4, and 5 min. As representative examples, SEM images of NWs after 3 min of growth revealed curved 2D NWs with nonconformal shells (Figure 3a, left), NWs with nonconformal shells on the curved outer surfaces of NWs along with conformal shells on relatively straight NW sections (Figure 3a, right), and straight NWs with conformal periodic shells (Supporting Information, Figure S2). The approximate yields of these three types of structures were 16, 22, and 62%, respectively. The curved, mixed curved/straight, and straight NW morphologies were observed for all times (representative SEM images, Supporting Information, Figures S3–S7), with relative yields of 24, 27, and 49%, respectively, at 15 s (Supporting Information, Figure S3), 23, 42, and 35%, respectively, at 30 s (Supporting Information, Figure S4), 13, 37, and 50%, respectively, at 1 min (Supporting Information, Figure S5), 16, 37, and 47%, respectively, at 4 min (Supporting Information, Figure S6), and 8, 31, and 61%, respectively, at 5 min (Supporting Information, Figure S7) growth.

A plot of the average lengths of nonconformal and conformal periodic Ge shells for each growth time (Figure 3b), and representative SEM images of nonconformal shells on curved cores for 0.25, 0.5, 1, 3 (Figures 3c–f) 4, and 5 min (Supporting Information, Figures S6 and S7) and on straight cores (Supporting Information, Figures S2–S7) for all times illustrate several key points. First, for short shell growth times the curved NW regions primarily had nonconformal Ge shells on the outside of the core, while straight sections had nonconformal shells alternating on opposite sides of the core (Supporting Information, Figures S3–S5). Second, for growth times of 1 min, the average length of nonconformal shells on the curved portion of the core is significantly greater than on the straight part of the core (Supporting Information, Figure S5). Third, for longer growth times ≥3 min, the nonconformal shells were observed on the outside of curved cores with average lengths increasing from ca. 2.3–4.2 μm, and much shorter conformal shells on ca. straight NW regions with average lengths increasing from ca. 165–250 nm. The average rates of growth of nonconformal and conformal Ge shells along the NW core are ca. 800 and 50 nm/min, respectively, as determined from the 3–5 min data. Fourth, the total number of

DOI: 10.1021/acs.nanolett.6b00629
Nano Lett. 2016, 16, 2830−2836

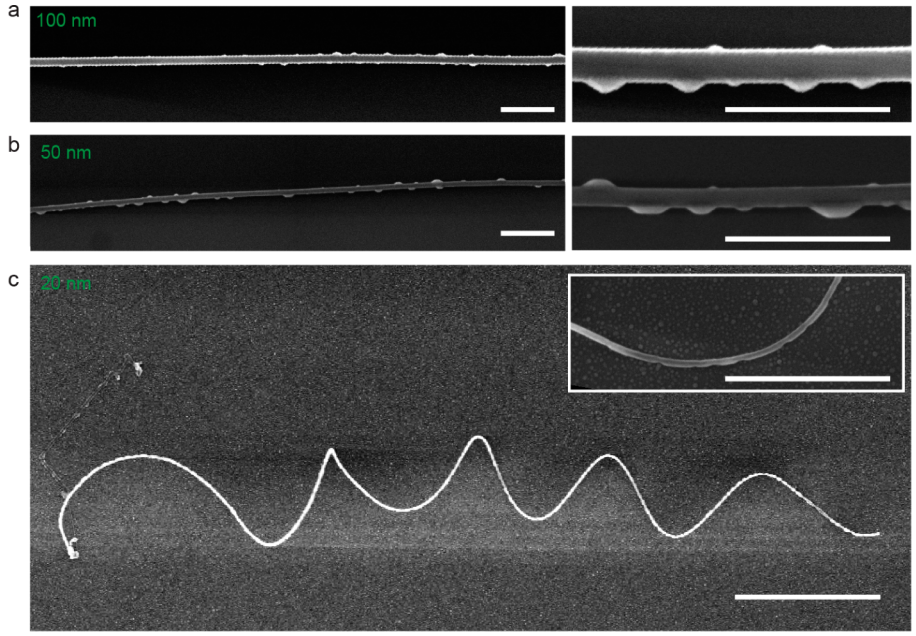

Figure 4. P-R crystal growth of Ge periodic shells on Si cores of different diameters. Ge was deposited at 520 °C with 40 sccm (19 mTorr) GeH_4 for 15−30 s. (a,b) SEM images of NWs after Ge was deposited on 100 nm (a) and 50 nm (b) Si cores. Scale bars: 500 nm. (c) SEM image of 3D spring obtained from growth on 20 nm Si core. Scale bar: 2 μm. Inset: Higher magnification SEM of 3D spring with one-sided Ge shells on the Si core. Scale bar: 500 nm.

nonconformal shells (Figures 3c−f) decreases over time, indicating that shells begin to merge at longer growth times. Taken together, these results show that nonconformal Ge shells remain nonconformal and grow more rapidly on the outer curved sections of the Si NW cores, while initially nonconformal shells grow more slowly on the straight portion of the NW and eventually become conformal.

To further investigate key factors controlling the growth of these interesting periodic structures we deposited Ge on different diameter Si NW cores for short times and characterized the corresponding NW morphologies. SEM images recorded following Ge shell growth at 520 °C with 40 sccm (19 mTorr) GeH_4 for 15−30 s on 100, 50, and 20 nm diameter Si NW cores (Figure 4) highlight several important points. The data from 100 and 50 nm cores (Figure 4a, b) showed nearly straight Si NWs. Higher magnification images (right, Figure 4a, b), show that many of the short nonconformal Ge shells grow on opposite sides of the NW cores in an ca. anticorrelated configuration. Anticorrelated arrangements of heterostructure islands were observed previously following the deposition of InAs onto 10−20 nm thick Si 2D membranes fabricated from silicon-on-insulator (SOI) wafers[39] and following deposition of Ge onto <25 nm thick 2D Si membranes and on 1D Si beams fabricated from SOI.[40] Anticorrelated patterns of Ge have also been observed after growth or annealing of Ge on Si NWs with diameters ≤100 nm.[30]

Notably, the growth on the smallest 20 nm cores revealed 2D spiral loop structures (Supporting Information, Figure S8) as well as 3D spring structures (Figure 4c) with yields of <10% for each structure. Higher magnification images of these 2D and 3D structures (Supporting Information, Figure S8 and Figure 4c inset) show that the majority of Ge shells grow on the outer curved side of the Si NW cores, similar to the 2D loop structures shown for 30 nm cores in Figures 2 and 3.

The 1D NW morphologies from Ge growth on 50 and 100 nm Si cores and the 3D spring morphologies from 20 nm cores can be understood by considering the Ge shell arrangements. As Ge shells are located on both sides of 50 and 100 nm cores, strain-induced bending on one side can oppose bending from the other side. This is also consistent with the 1D morphologies of Figure 1, which have radially conformal shells on 50 nm cores. Furthermore, comparing morphologies from short growth times (Figure 4) with long times (Figure 1) on 50 nm cores suggests that isolated and/or anticorrelated shells develop into radially conformal ones. For 3D springs from growth on 20 nm cores, Ge shells lie on the outside of the core, which induces bending away from the shells similar to 2D loops for 30 nm cores. Previous reports[41] showed how 2D spirals and 3D springs can relieve strain from biaxially stressed materials fabricated by top-down lithographic methods, where the formation of a specific morphology depended on the thickness and dimensions of the two layers. 3D springs allow strain to be shared evenly over the length of the core, as the radius of curvature for each rotation is the same along its length. Alternatively, for a 2D spiral, each loop has an increasing radius of curvature with every rotation in order for the structure to maintain a flat, 2D geometry,[41] which is consistent with our observed morphology for 2D spirals obtained from growth on 20 nm Si cores (Supporting Information Figure S8). Taken together, these results show that the likelihood of obtaining one-sided growth increases as core diameter decreases and that 2D spirals and 3D springs are alternative morphologies for strain relaxation in addition to 2D loops.

We now consider a model for the nonconformal growth of Ge periodic shells on Si NWs by combining our homoepitaxial P-R crystal growth concepts[23] with heteroepitaxial strain and the flexible freestanding NW substrates. First, we assume that an initial periodic Ge shell grows on one side of a Si NW, which generates a strain shared between the core and shell. Tensile Si strain at the Si/Ge interface induces bending, which

DOI: 10.1021/acs.nanolett.6b00629
Nano Lett. 2016, 16, 2830−2836

compressively strains the Si surface opposite to the heterointerface. Second, we suggest that this bending-induced strain alters the surface energetics for subsequent growth. Specifically, after forming the initial periodic Ge shell on one side of the core, subsequent Ge nucleation and growth can be promoted on the same side and suppressed on the opposite. This serves as positive feedback to produce highly ordered configurations, such as 2D loops or 3D springs, where the majority of shells form on the same side of the NW. Last, in the P-R crystal growth regime where we are growing shells, we propose that the relatively long surface diffusion lengths provide kinetic access to this strain-mediated growth of curved morphologies on compliant freestanding NW substrates.

The three parts of our model are consistent with literature, our observations, and additional experiments. First, reports have shown how strain from Ge or InAs island growth can be shared with thin, compliant Si substrates.[35,36,38,39] This strain induces bending of the substrate and can create a "global" substrate strain even away from the "local" strain at the island/substrate interface.[39] We do not observe 2D loop structures without Ge growth, supporting the idea that nonconformal shells transfer strain to and induce bending of our NW substrates. Furthermore, additional growth studies (e.g., Supporting Information Figure S9) where Ge was deposited on 30 nm Si cores at lower pressures compared to data in Figure 3 clearly illustrate the "local" strain at the Ge/Si interface and provide evidence for a "global" strain of the NW substrate between Ge shells. Second, heterogrowth on strained or curved substrates has been shown to deviate from growth on bulk, flat substrates[35−40] because surface diffusion lengths and nucleation rates are influenced by the strain energy and curvature of surfaces.[36−38] The growth dynamics of our nonconformal shells on curved cores (Figure 3) are consistent with a strain-mediated mechanism. As shown in Figure 3c, Ge nucleation and growth can occur on one-side of a straight Si NW in less than 15 s. Even after an additional 45 s (Figure 3e), Ge is not observed on the Si surface opposite the curved Si/Ge interface, and the nonconformal shells on the curved cores are notably longer than the nonconformal shells on straight cores (Supporting Information, Figure S5). Furthermore, shells on curved cores remain nonconformal even for long times (Figure 3) and grow an order of magnitude faster than conformal shells on straight cores (Figure 3b). Together, these results suggest strongly that initial Ge shell growth modifies the surface chemistry and growth dynamics by suppressing subsequent Ge growth on the opposite compressively strained surface, and promoting growth on the same tensile strained surface (for our low pressure growth conditions).

Last, in order to initiate one-sided growth, we propose that growth of the initial shell must generate a "critical" amount of strain so that subsequent growth is suppressed on the Si surface opposite the heterointerface. If subsequent growth occurs in a random or anticorrelated configuration before this "critical" strain is achieved, then one-sided growth may not proceed. One-sided growth should be easier (1) with smaller NW cores because the shell thickness needed to reach a certain level of strain from bending decreases with diameter[33] and (2) with conditions where nucleation rates are slow (see Supporting Information for further discussion). Consistent with this hypothesis, initial growth on 50 and 100 nm cores yields mostly anticorrelated Ge shells, 30 nm cores yield anticorrelated shells as well as 2D loops with same-sided shells, especially near the freestanding NW tip, and 20 nm cores yield 2D loops and 3D springs with same-sided shells. Furthermore, the variation in size and density of anticorrelated Ge shells along 100 and 50 nm cores (Figure 4) suggest that nucleation and growth does not occur at the same time along the NW. Finally, prior reports[34] of Ge deposition at 380 °C and 0.4 Torr on 20−30 nm Si cores resulted in uniform-diameter, radially conformal shells that were continuous along the core. As discussed previously, our lower pressures and higher temperature conditions increase diffusion lengths, allowing material to concentrate into fewer, larger periodic shell islands in order to reach lower thermodynamic free-energy states consistent with the P-R crystal structure and minimization of the heteroepitaxial strain.

In conclusion, we have described new P-R crystal growth studies of heterostructures in which Ge (Si) is deposited on Si (Ge) 1D cores to generate complex NW morphologies in 1, 2, or 3D. Depositing Ge on 50 nm Si cores yields a single set of periodic shells, while sequential variation of GeH_4 pressure can yield multimodulated 1D NWs with distinct sets of shell periodicities. P-R crystal growth on more flexible 30 nm cores produces 2D loop structures, where Ge (Si) shells lie primarily on the outside (inside) of highly curved Si (Ge) cores. Systematic investigation of shell morphology as a function of growth time indicates that Ge shells grow 10 times faster in length along positive curvature Si cores than along straight Si cores. Short Ge deposition times further reveal that shells develop on opposite sides of 50 and 100 nm Si cores to form straight 1D morphologies but that shells develop on the same side of 20 nm cores to produce 2D loop and 3D spring structures. In addition, we have developed a model to explain, in general, the potential of heteroepitaxial growth in the P-R crystal growth regime. Our model suggests several promising areas for future exploration, including (1) growth of heterostructures with even greater lattice mismatch and (2) heteroepitaxial growth on smaller diameter NWs, which could accommodate additional strain through greater bending and/or by reducing the heterointerface area. Last, long nonconformal shells on 1D substrates may represent a new type of freestanding quantum dot/wire structure, where the quantum dot/wire width is determined by the NW core, and the quantum dot size and spacing along the NW axis can be tuned through synthesis.

■ ASSOCIATED CONTENT

Supporting Information

The Supporting Information is available free of charge on the ACS Publications website at DOI: 10.1021/acs.nanolett.6b00629.

Detailed description of experimental methods and additional figures (PDF)

■ AUTHOR INFORMATION

Corresponding Author

*E-mail: cml@cmliris.harvard.edu.

Notes

The authors declare no competing financial interest.

■ ACKNOWLEDGMENTS

The authors gratefully acknowledge A. Magyar for assistance with electron microscopy and Hitachi for STEM use; R.W.D acknowledges a NSF Graduate Research Fellowship; M.N.M. acknowledges a Fannie and John Hertz Foundation Graduate

DOI: 10.1021/acs.nanolett.6b00629
Nano Lett. 2016, 16, 2830−2836

Fellowship and a NSF Graduate Research Fellowship. This work was performed in part at the Center for Nanoscale Systems (CNS), a member of the National Nanotechnology Infrastructure Network (NNIN), which is supported by the National Science Foundation under NSF award no. ECS-0335765. CNS is part of Harvard University.

REFERENCES

(1) Hu, J. T.; Odom, T. W.; Lieber, C. M. *Acc. Chem. Res.* **1999**, *32*, 435−445.
(2) Lieber, C. M. *MRS Bull.* **2011**, *36*, 1052−1063.
(3) Xia, Y. N.; Yang, P. D.; Sun, Y. G.; Wu, Y. Y.; Mayers, B.; Gates, B.; Yin, Y. D.; Kim, F.; Yan, Y. Q. *Adv. Mater.* **2003**, *15*, 353−389.
(4) Dasgupta, N. P.; Sun, J. W.; Liu, C.; Brittman, S.; Andrews, S. C.; Lim, J.; Gao, H. W.; Yan, R. X.; Yang, P. D. *Adv. Mater.* **2014**, *26*, 2137−2184.
(5) Kempa, T. J.; Day, R. W.; Kim, S.-K.; Park, H.-G.; Lieber, C. M. *Energy Environ. Sci.* **2013**, *6*, 719−733.
(6) Brongersma, M. L.; Cui, Y.; Fan, S. *Nat. Mater.* **2014**, *13*, 451−460.
(7) Cartoixa, X.; Colombo, L.; Rurali, R. *Nano Lett.* **2015**, *15*, 8255−8259.
(8) Lin, D.; Fan, P.; Hasman, E.; Brongersma, M. L. *Science* **2014**, *345*, 298−302.
(9) Luo, Z. Q.; Jiang, Y. W.; Myers, B. D.; Isheim, D.; Wu, J. S.; Zimmerman, J. F.; Wang, Z. A.; Li, Q. Q.; Wang, Y. C.; Chen, X. Q.; Dravid, V. P.; Seidman, D. N.; Tian, B. Z. *Science* **2015**, *348*, 1451−1455.
(10) Duan, X.; Lieber, C. M. *Nano Res.* **2015**, *8*, 1−22.
(11) Mourik, V.; Zuo, K.; Frolov, S. M.; Plissard, S. R.; Bakkers, E. P. A. M.; Kouwenhoven, L. P. *Science* **2012**, *336*, 1003−1007.
(12) Deshpande, V. V.; Bockrath, M.; Glazman, L. I.; Yacoby, A. *Nature* **2010**, *464*, 209−216.
(13) Schmidt, V.; Wittemann, J. V.; Gosele, U. *Chem. Rev.* **2010**, *110*, 361−388.
(14) Hauge, H. I. T.; Verheijen, M. A.; Conesa-Boj, S.; Etzelstorfer, T.; Watzinger, M.; Kriegner, D.; Zardo, I.; Fasolato, C.; Capitani, F.; Postorino, P.; Kolling, S.; Li, A.; Assali, S.; Stangl, J.; Bakkers, E. P. A. M. *Nano Lett.* **2015**, *15*, 5855−5860.
(15) Panciera, F.; Chou, Y.-C.; Reuter, M. C.; Zakharov, D.; Stach, E. A.; Hofmann, S.; Ross, F. M. *Nat. Mater.* **2015**, *14*, 820−825.
(16) de la Mata, M.; Zhou, Xi.; Furtmayr, F.; Teubert, J.; Gradečak, S.; Eickhoff, M.; Fontcuberta i Morral, A.; Arbiol, J. *J. Mater. Chem. C* **2013**, *1*, 4300−4312.
(17) Tian, B. Z.; Xie, P.; Kempa, T. J.; Bell, D. C.; Lieber, C. M. *Nat. Nanotechnol.* **2009**, *4*, 824−829.
(18) Musin, I. R.; Filler, M. *Nano Lett.* **2012**, *12*, 3363−3368.
(19) Caroff, P.; Dick, K. A.; Johansson, J.; Messing, M. E.; Deppert, K.; Samuelson, L. *Nat. Nanotechnol.* **2009**, *4*, 50−55.
(20) Lim, S. K.; Crawford, S.; Haberfehlner, G.; Gradečak, S. *Nano Lett.* **2013**, *13*, 331−336.
(21) Musin, I. R.; Boyuk, D. S.; Filler, M. A. *J. Vac. Sci. Technol. B* **2013**, *31*, 020603.
(22) Christesen, J. D.; Pinion, C. W.; Grumstrup, E. M.; Papanikolas, J. M.; Cahoon, J. F. *Nano Lett.* **2013**, *13*, 6281−6286.
(23) Day, R. W.; Mankin, M. N.; Gao, R.; No, Y.-S.; Kim, S.-K.; Bell, D. C.; Park, H.-G.; Lieber, C. M. *Nat. Nanotechnol.* **2015**, *10*, 345−352.
(24) Oliveira, D. S.; Tizei, L. H. G.; Ugarte, D.; Cotta, M. A. *Nano Lett.* **2013**, *13*, 9−13.
(25) Smith, D. L. *Thin-Film Deposition: Principles & Practice*; McGraw-Hill: New York, 1995.
(26) Lu, W.; Xiang, J.; Timko, B.; Wu, Y.; Lieber, C. M. *Proc. Natl. Acad. Sci. U. S. A.* **2005**, *102*, 10046−10051.
(27) Li, J.; Shan, Z.; Ma, E. *MRS Bull.* **2014**, *39*, 108−114.
(28) Goldthorpe, I. A.; Marshall, A. F.; McIntyre, P. C. *Nano Lett.* **2008**, *8*, 4081−4086.
(29) Schmidt, V.; McIntyre, P. C.; Gosele, U. *Phys. Rev. B: Condens. Matter Mater. Phys.* **2008**, *77*, 235302.
(30) Kwon, S.; Chen, Z. C. Y.; Kim, J.-H.; Xiang, J. *Nano Lett.* **2012**, *12*, 4757−4762.
(31) Pan, L.; Lew, K.-K.; Redwing, J. M.; Dickey, E. C. *Nano Lett.* **2005**, *5*, 1081−1085.
(32) Tallinen, T.; Chung, J. Y.; Rousseau, F.; Girard, N.; Lefevre, J.; Mahadevan, L. *Nat. Phys.* **2016**, DOI: 10.1038/nphys3632.
(33) Li, X.-F.; Wang, B.-L.; Lee, K. Y. *J. Appl. Phys.* **2009**, *105*, 074306.
(34) Lauhon, L. J.; Gudiksen, M. S.; Wang, D.; Lieber, C. M. *Nature* **2002**, *420*, 57−61.
(35) Huang, M.; Ritz, C. S.; Novakovic, B.; Yu, D.; Zhang, Y.; Flack, F.; Savage, D. E.; Evans, P. G.; Knezevic, I.; Liu, F.; Lagally, M. G. *ACS Nano* **2009**, *3*, 721−727.
(36) Gill, S. P. A. *Appl. Phys. Lett.* **2011**, *98*, 161910.
(37) Yang, B.; Liu, F.; Lagally, M. G. *Phys. Rev. Lett.* **2004**, *92*, 025502.
(38) Kim-Lee, H.-J.; Savage, D. E.; Ritz, C. S.; Lagally, M. G.; Turner, K. T. *Phys. Rev. Lett.* **2009**, *102*, 226103.
(39) Deneke, C.; Malachias, A.; Rastelli, A.; Merces, L.; Huang, M.; Cavallo, F.; Schmidt, O. G.; Lagally, M. G. *ACS Nano* **2012**, *6*, 10287−10295.
(40) Ritz, C. S.; Kim-Lee, H.-J.; Detert, D. M.; Kelly, M. M.; Flack, F.; Savage, D. E.; Cai, Z.; Evans, P. G.; Turner, K. T.; Lagally, M. G. *New J. Phys.* **2010**, *12*, 103011.
(41) Huang, M.; Boone, C.; Roberts, M.; Savage, D. E.; Lagally, M. G.; Shaji, N.; Qin, H.; Blick, R.; Nairn, J. A.; Liu, F. *Adv. Mater.* **2005**, *17*, 2860−2864.

DOI: 10.1021/acs.nanolett.6b00629
Nano Lett. 2016, 16, 2830−2836